Results in Engineering 8 (2020) 100164

Contents lists available at ScienceDirect

Results in Engineering

journal homepage: www.editorialmanager.com/rineng/Default.aspx

Numerical and analytical investigations on projectile perforation on steel–concrete–steel sandwich panels

Jun Feng [a], Weibing Li [b,*], Chufan Ding [a], Dacheng Gao [b], Ze Shi [b,c], Jianguo Liang [d,**]

[a] National Key Laboratory of Transient Physics, Nanjing University of Science and Technology, Nanjing, 210094, China
[b] School of Mechanical Engineering, Nanjing University of Science and Technology, Nanjing, 210094, China
[c] State Key Laboratory of Explosion Science and Technology, Beijing Institute of Technology, Beijing, 100081, China
[d] College of Mechanical and Vehicle Engineering, Taiyuan University of Technology, Taiyuan, 030024, China

ARTICLE INFO

Keywords:
SCS sandwich panels
FE simulation
Cavity expansion analysis
Petalling of steel plates
Energy consumption

ABSTRACT

Steel–concrete–steel (SCS) sandwich panels have been achieving increasing attention due to its good impact resistant performance, but there still lacks related research concerning analytical model for SCS perforation. In this paper, numerical and analytical investigations were performed to study the impact resistance of SCS sandwich panels against rigid projectile penetration. FE simulations of concrete-steel perforation were conducted to validate the numerical model in terms of projectile residual velocity and damage mode. With same concrete core, five thickness combinations of front and rear steel plates were numerically studied to explore the sandwich structural effect on the perforation responses. Utilizing spherical cavity expansion analysis and plates petalling theory, a semi-empirical analytical model was developed to describe the perforation on SCS sandwich panels, which was characterized with 7 penetration stages. Agreement was reached between numerical simulation and theoretical model in terms of both projectile deceleration history and residual velocity. On the perspective of structurally absorbed energy, the thickness combinations of front and rear steel plate were further analyzed and discussed. For the same thickness, the rear steel plate was found to consume more energy than the front plate, which provides better protection against projectile impact loadings.

1. Introduction

For sandwich wall structures, one of the most obvious advantages is less use of material for better mechanical performance [1–3]. Due to excellent bearing capacity, excellent impermeability and convenience of construction, the steel–concrete–steel (SCS) sandwich panels have been widely used in nuclear power plant, high-rise buildings, offshore structures and fortifications [4,5]. Consisting of a concrete core connected to two steel plates, SCS sandwich panels were originally conceived during the initial design stages for the Convy River submerged tube tunnel in the UK [6].

In recent decades, many scholars have investigated the performance of SCS sandwich wall structures and large variety of sandwich structures have been applied in structural engineering [1,7]. Furthermore, SCS sandwich panels have a good performance in resisting dynamic loadings including penetration and explosion. Under projectile impact, concrete panel usually suffers reflected tensile stress wave induced fracture owning to its brittleness [8,9]. The confinement on the front and rear free surface of the concrete panel may strengthen the structure against impactive loadings [10]. The local failure mode of SCS sandwich panels under projectile impact differs from monolithic concrete panel, because the steel plates pose a significant influence on cater forming and preventing the pulverized concrete pieces flying away [2,11].

There have been a few studies shedding some light on the mechanical performance of concrete-steel composite under dynamic conditions. Without shear connectors connecting steel faceplates and concrete core, the design concept of non-composite SCS sandwich panels were presented by Crawford and Lan [4] to resist blast loading which provided experimental verification for the full-scale blast wall. Remennikov et al. [5,12] investigated both static and impact performance of non-composite SCS panels whereas the tested panels exhibited tensile membrane resistance at large deformation. Bruhl et al. [13] came up with a three-step method for designing steel-plate concrete walls against missile impact. This method could be used to evaluate the minimum required steel plate thickness of steel plate composite (SC) walls to prevent perforation. Kim

* Corresponding author.
** Corresponding author.
E-mail addresses: jun.feng@njust.edu.cn (J. Feng), njustlwb@163.com (W. Li), liangjianguo20@hotmail.com (J. Liang).

https://doi.org/10.1016/j.rineng.2020.100164
Received 15 June 2020; Received in revised form 24 July 2020; Accepted 12 August 2020

Nomenclature

A_1	Empirical factor
b	Thickness of steel plate
b_1	Thickness of front steel plate
b_2	Thickness of rear steel plate
c	Empirical factor
d	Perforation distance in rear steel plate
D	Diameter of projectile nose
E	Young's modulus
E_c	Minimum perforation energy
$f_c^{'}$	Unconfined cylinder compressive strength of concrete
F	Resistant force
F_{mean}	Mean resistant force
h	Length of projectile nose
h_c	Thickness of concrete slab
$H_{p,f}$	Depth of front crater
$H_{p,r}$	Depth of rear crater
k	Slope of curve
M_0	Mass of projectile
p	Hardening exponent
R	Impact toughness
s	Area of nose surface
S	Dimensionless constant
v	Normal velocity of nose surface
V	Velocity
V_s	Striking velocity
V_r	Residual velocity
$V_{r,n}$	Residual velocity of numerical model
$V_{r,a}$	Residual velocity of analytical model
W_L	Local energy consumption
W_G	Plastic deformation energy of remaining part
Y	Yield strength of front steel plate
α	Constant
β	Constant
δ_t	Crack tip opening displacement parameter (CTOD)
$\overline{\delta}$	Dimensionless CTOD parameter
υ	Poisson's ratio
ρ	Density
ρ_t	Density of steel plate
σ_0	Flow stress
σ_n	Normal resistant stress
$\sigma_{n,b_1}^{'}$	Normal resistance of front steel plate
$\sigma_{n,c}$	Normal resistance of concrete slab
$\sigma_{n,c}^{'}$	Normal resistance of pulverized concrete
σ_u	Ultimate strength of the steel
σ_y	Yield stress of rear steel plate
ϕ	Empirical constant

et al. [14] conducted a preliminary study on the local impact behavior of SC walls to comprehensively investigate the dynamic characteristics of steel-concrete walls under local impact conditions. Feng et al. [15] dealt with the dynamic response of a double-layered target of concrete and armour steel subjected to projectile impact, implying that the spaced targets have a greater residual penetration depth than segmented targets. Conducting a series of drop hammer impact tests and axial compression tests, Zhao and Guo [16] studied impact and post-impact behavior of steel-concrete composite panels to develop the empirical model for residual strength evaluation. It was found that the axial compressive preload could be beneficial to resist the impact loadings.

Although dynamic impact responses of SCS structures have been extensively studied through experiments, there still lacks analytical model for projectile perforation on SCS panels. The role of front and rear steel plate played on energy consumption is not clear either. The knowledge gap hinders the engineering application of such SCS sandwich structure for shelter construction. Although the perforation analysis has been developed based on energy conservation, the projectile deceleration history during perforation cannot be obtained. The analytical model of dynamic response of projectile perforation in terms of explicit form resistant force is thus needed.

Using the non-linear transient dynamic finite element solver LS-DYNA, this work adopted 3 dimensional finite element modeling to analyze SCS sandwich panels with no shear connecting steel faceplates and concrete. By keeping constant total thickness of steel plates, we examined the influence of steel plates by changing the thickness combinations of front and rear steel plates. Finally, a simple but effective semi-empirical analytical model for residual velocity prediction was put forward and validated. The results may shed some light on SCS sandwich structure design with better impact resistance performance.

2. Penetration model validation

Prior to numerical analysis of SCS panels, the FE model for penetration on concrete and steel targets needs to be developed and validated. Wu et al. [8] experimentally investigated hard projectile perforation on the reinforced concrete (RC) panels with a rear steel liner, which is similar to the interested SCS sandwich panels. This work adopted these experiments to validate the FE numerical model for perforation of SCS sandwich panels.

2.1. FE model for SC perforation

The ogival nose projectiles used in the experiments were machined

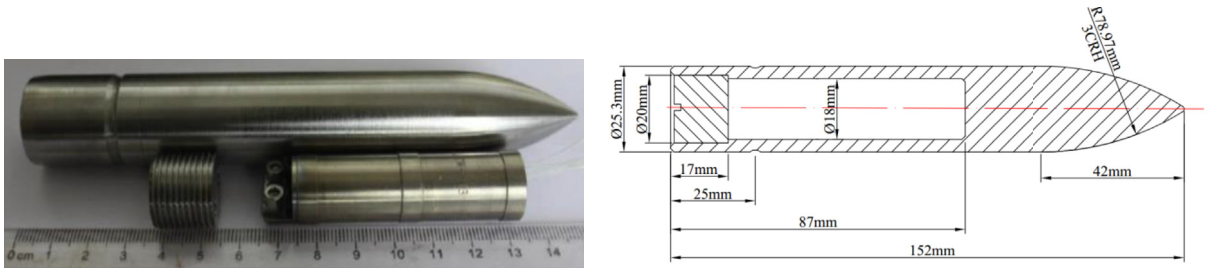

(a) Photograph (b) Geometric dimension

Fig. 1. Projectile and dimensions.

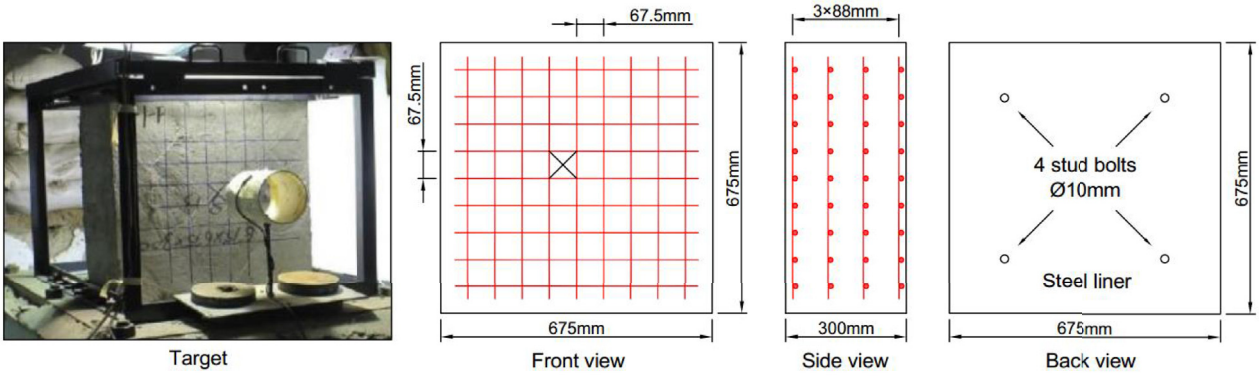

Fig. 2. Geometric dimensions of target.

Table 1
Model parameters for concrete (units: cm-g-μs).

RO	G	A	B	C	N	FC	T	EPSO	EFMIN
2.24	0.1486	0.79	1.6	0.007	0.61	4.1e-4	4.1e-5	1e-6	0.01
SFMAX	*PC*	*UC*	*PL*	*UL*	D_1	D_2	K_1	K_2	K_3
7.0	1.6e-4	0.001	0.008	0.1	0.04	1.0	0.85	−1.71	2.08

Table 2
Model parameters for steel liner (units: cm-g-μs).

RO	G	A	B	N	C	M	TM	TR	EPSO
7.896	0.818	3.5e-3	2.75e-03	0.36	0.22e-01	1	1793	293	1e-6
CP	*PC*	*SPALL*	*IT*	D_1	D_2	D_3	D_4	D_5	*C2/P*
0.452e-5	0	2	0	−0.8	2.1	−0.5	0.0002	0.61	1

from 45CrNiMoV steel rods and heat treated to a hardness of HRC45 with yield strength of 1420 MPa. The mass of projectile and the accelerometer were 386 g and 42 g, respectively. The photograph and detailed dimensions of the projectile were shown in Fig. 1.

This paper chose to simulate the penetration tests with 300 mm thickness RC panels whereas the concrete thickness is chose to the practical shear wall. Fig. 2 depicted the target dimension and the locations of its reinforced mesh. 4 layers of two-way square-pattern steel mesh were incorporated where 9 bars with 6 mm diameter were arranged in each direction, and concrete cover was about 15 mm in-depth. A steel

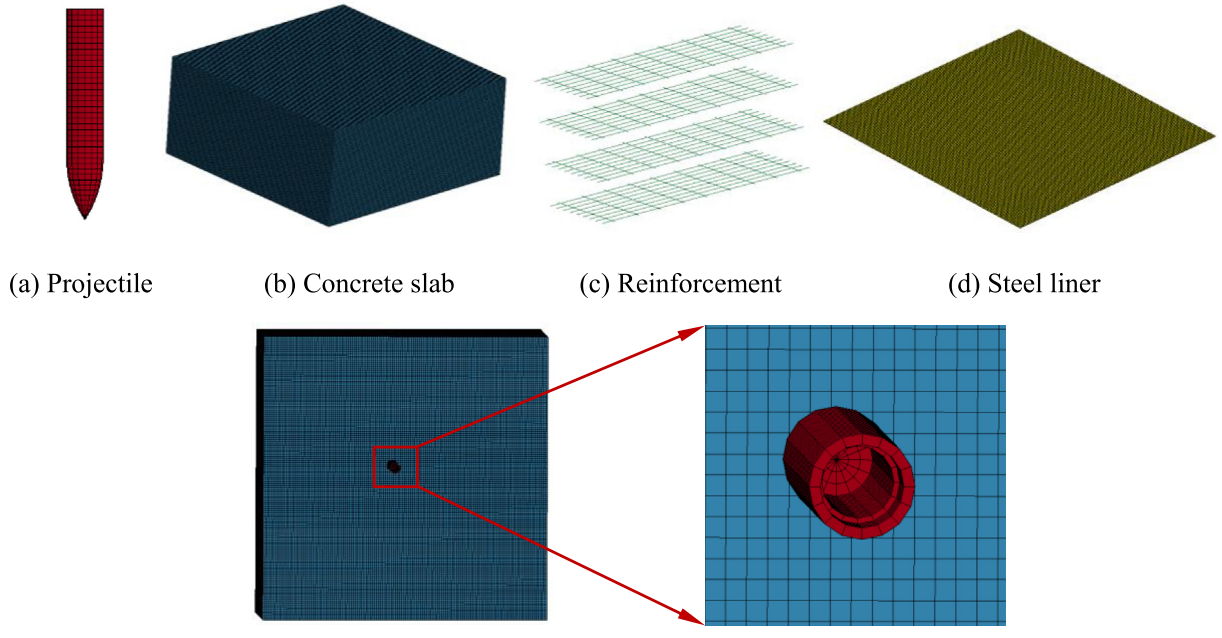

Fig. 3. Finite element model for projectile perforation on RC panel with steel liner.

Table 3
Number of elements for every part.

Part	Projectile	Concrete slab	Reinforced rebars	Steel liner
Number of elements	800	1,822,500	8712	18,496

plate with 1 mm thickness was welded by four stud bolts onto the rear face of the RC panel. The impact point of projectile was denoted by "×". The unconfined cylinder compressive strength of 15 cm cubic concrete specimens was 41 MPa.

For this penetration tests, the projectile did not hit the reinforcment layers. For 0.5% reinforcement mesh ratio in the investigated tests, the reinforcement mesh has little effect on the terminal ballistic parameters [17,18]. After penetration, it was found that the blunted lengths and mass losses of projectiles were less than 3.3% and 2.5%, respectively. Therefore, the penetrator of 430 g including projectile and accelerator, could be regarded as rigid body suffering no deformation and erosion for the sequent simulations [19].

Due to the lack of detailed information of the SC composite target perforation, the imperfections of specimen geometry and boundary conditions were not considered herein. Although geometric imperfection may have some effects in structural load carrying capacity according to Ref. [20–22], the projectile penetration and perforation work usually ignore such details [14–16]. Hence, the ideal hard projectile normal impact on edge fixed composite targets was studied.

The widely used explicit solver LS-DYNA was adopted for the penetration simulation whereby 3D solid 164 element was selected to model projectile, concrete slab and steel liner, and element type of the steel mesh was 3D beam 161. The projectile was modelled as a rigid body described by MAT_RIGID in LS-DYNA [23,24]. The Holmquist-Johnson-Cook (HJC) model [25], which has been extensively applied for concrete penetration simulations, was selected to describe the concrete material. The steel liner was modelled by Johnson-Cook (JC) model [26] for its wide adoption in viscoplastic domain. With reference to Zhao et al. [27], the steel mesh was described by MAT_PLASTIC_KINEMATIC. Parameters for HJC model and JC model of #1006 steel were listed in Tables 1 and 2 which have been verified against some available penetration tests [28–30]. According to the experimental setup, fixed boundary conditions were applied to all the upper and lower surfaces of the target. To ensure the nodes of steel mesh coinciding with concrete element nodes, the element sizes were strictly controlled where the minimum element size is 3 mm for both projectiles and concrete slab. The interactions between the projectile, concrete slab and steel liner were modelled with surface to surface eroding algorithms. A maximum principal strain at failure for concrete was set as the element erosion criteria using MAT_ADD_EROSION. The developed finite element model, including projectile, concrete, reinforcement and steel plate, for penetration test was shown in Fig. 3. Finally, element numbers of four parts, i.e., projectile, concrete slab, steel mesh and steel liner, were given in Table 3.

2.2. Numerical results discussion

For different striking velocities (V_s), five penetration simulations were performed to validate the numerical model. The projectile residual velocities of the experiment ($V_{r,e}$) and numerical simulation ($V_{r,n}$) were compared in Fig. 4(a) where the numerical residual velocities agreed well with the experimental data with maximum error ($(V_{r,n} - V_{r,e})/(V_s - V_{r,e})$) less than 4%. It was indicated that the projectile with 540 m/s striking velocity could not perforate the target and the depth of penetration (DOP) was 254 mm. The numerical DOP was calculated as 261 mm, also matching test data well. Projectile velocity evolution during perforation was exhibited in Fig. 4(b). It was implied that the higher projectile striking velocity corresponds to less penetration time. For the projectile with a striking velocity of 540 m/s, it failed to perforate the target and stayed in the target eventually. Moreover, the depths of front crater and rear crater could be predicted by the numerical model, which were compared with test data in Table 4 suggesting the rear crater is deeper than front crater.

Fig. 5 compared numerical damage modes with post-test target photo in different views. The actual destructive mode of rear surface of the target was shown in Fig. 5(a) while Fig. 5(b) depicted the deformation of the steel liner which was notable that the neighbor region of the liner

Table 4
Perforation results of simulation and test.

V_s(m/s)	$V_{r,e}$(m/s)	$V_{r,n}$(m/s)	Error	$H^e_{p,f}/H^n_{p,f}$(mm)	$H^e_{p,r}/H^n_{p,r}$(mm)
540	0	0	\	55/40	\
601	180	192	+2.85%	60/48	70/66
641.5	272	264	−2.17%	55/48	55/78
679	329	318	−3.14%	60/40	65/64
737	422	417	−1.59%	57/50	60/78

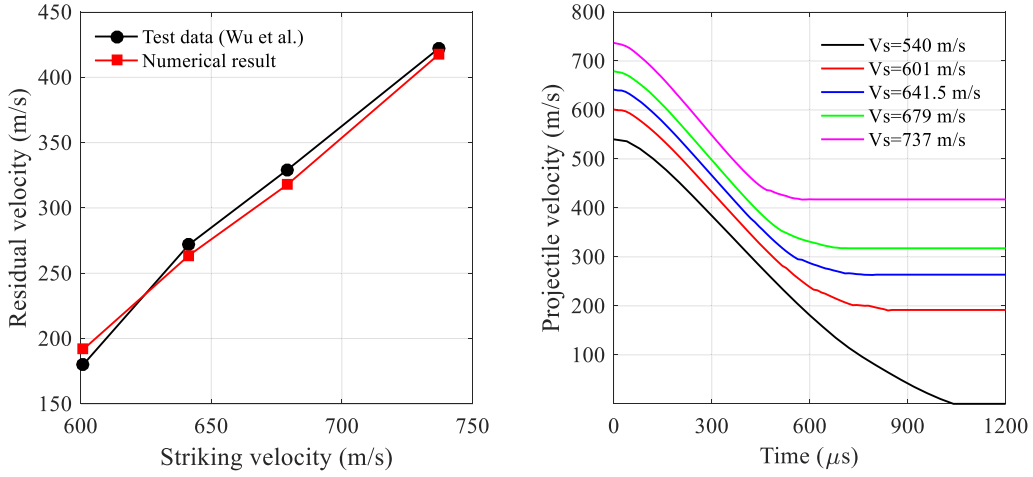

(a) Comparison between experiment and simulation (b) Projectile velocity evolution over time

Fig. 4. Numerical model validation against experimental results.

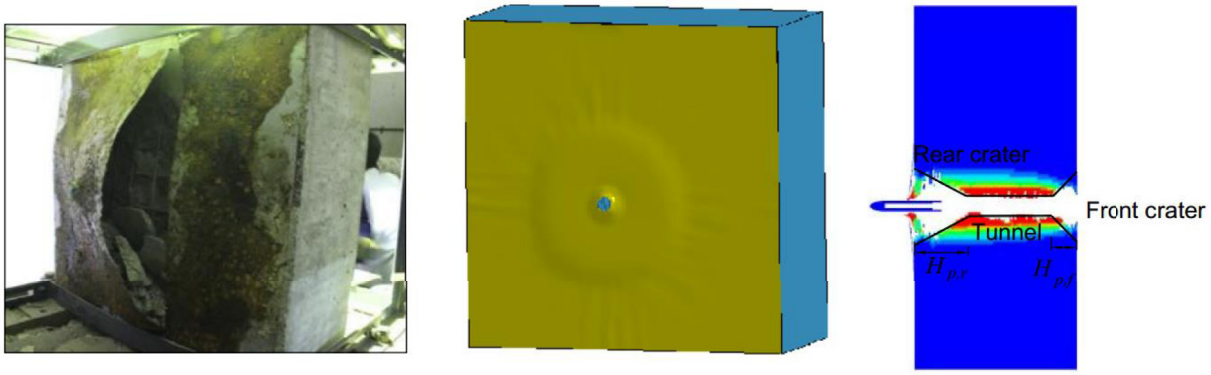

(a) Rear target (b) Steel liner deformation (c) Cross-section view

Fig. 5. The damaged contour of target.

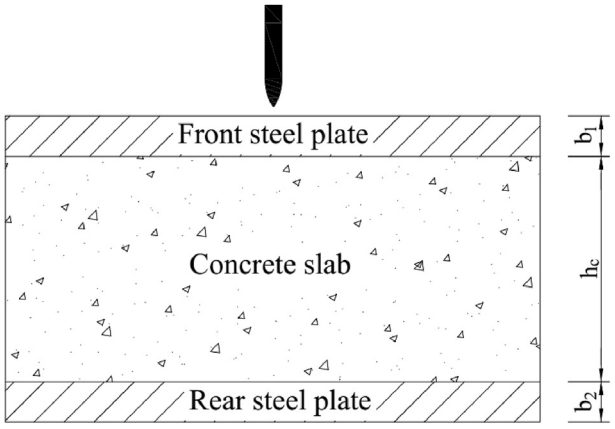

Fig. 6. Schematic diagram of SCS sandwich panels under projectile impact.

around the projectile deformed severer. For the cross-section view, Fig. 5(c) showed the damage mode of the target corresponding to the three-stage perforation model [18] which consists of front impact crater, ballistic tunnel (with almost same diameter with projectile shank), and a nearly frustum-of-cone shaped rear crater was numerically verified. In terms of destructive forms and residual velocity, the numerical model had a good consistency with concrete-steel perforation tests, ensuring the feasibility of the sequent penetration modeling of SCS sandwich panels.

3. Numerical study of perforation on SCS sandwich panels

This section aims to model the non-composite SCS sandwich panels against the projectile impact with its schematic diagram shown in Fig. 6. The SCS sandwich panels, with different thickness combinations of front and rear steel plates, were extensively studied for the purpose of structural optimization.

3.1. Modeling scheme

The simulation scheme of the SCS sandwich panels were as follows: the foregoing projectile without the acceleration sensor was used here as penetrator and the mass and density of projectile were 340 g and 7.83 g/cm^3. With 800 mm × 800 mm section, the investigated panel structures were studied with 2–10 mm thickness for both front and rear steel plates. In particular, the total thickness of the front and rear steel plates remained 12 mm, i.e., $b_1 + b_2 = 12\,mm$. Hence, there were 5 kinds of combinations, e.g., 2-10, 4-8, 6-6, 8-4 and 10-2 where "-" represented the thickness combination of front and rear steel plates. For same square dimension, the thickness of concrete slabs was selected as 200, 250 and 300 mm, respectively. For the SCS sandwich panels with 300 mm thickness concrete slab, the striking velocity of the projectile was designed as 650, 675, 700 and 720 m/s. For the cases with 200 and 250 mm thickness concrete slabs, the striking velocity of 675 m/s was used for perforation simulation. All impact points were located at the center of the targets.

For the SCS sandwich panels, all the components were explicitly modelled in three dimensions. For computational efficiency, the FE models were created as quarter symmetric bodies with symmetric boundary condition where the grids near contact region were refined. Fig. 7 gave an overview of the FE model and mesh details. Suitable mesh size was chosen to ensure the convergence of numerical results of the SCS sandwich panels perforation whereas the minimum element size is 3 mm for both projectiles and targets. For the 1/4 model of SCS sandwich panels with combination of 2–10 steel plates and 200 mm thickness concrete slab, the numbers of elements of four parts were listed in

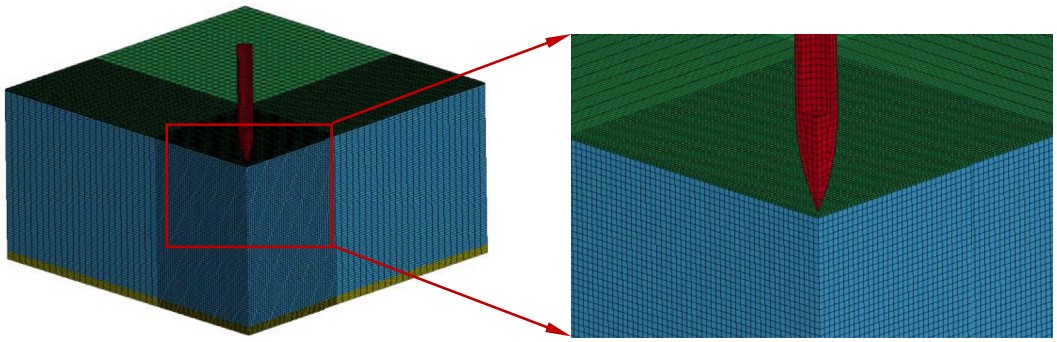

Fig. 7. Overview of the perforation FE model.

Table 5
Number of elements for every part.

Part	Projectile	Concrete	Front steel plate	Rear steel plate
Number of elements	696	376,875	20,000	50,000

Table 5. Similarly, 3D solid 164 element was selected to model these four parts and the projectile was also described by MAT_RIGID. These models and parameters of concrete slab and steel plates were same as foregoing model. All the interactions among the projectile, concrete slab and steel liner were modelled with surface to surface eroding algorithms. A maximum principal strain at failure for concrete was set as the element erosion criteria using MAT_ADD_EROSION. To simulate the semi-infinite target, no reflection boundary conditions were applied to the SCS sandwich panels. At the beginning of each simulation, the projectile was placed 1 mm away from target front surface and given an initial normal velocity.

3.2. Discussion of SCS sandwich panels perforation

To examine the impact resistance of SCS panels under different striking velocities, this section numerically studied the 200, 250 and 300 mm thickness concrete slab pinched by different thickness front and rear steel plates. Under various striking velocities, the different combinations of front and rear steel plates were supposed to have some effects on the projectile residual velocity. 30 kinds of thickness combinations were selected for the analysis of SCS sandwich panels. The numerical results of SCS sandwich panels with 200 mm thickness concrete slab and 2-10 steel plates were demonstrated in Fig. 8. The projectile with striking velocity of 675 m/s perforated the SCS sandwich panels as expected. The damaged area of the rear steel plate was larger than the front steel plate because of the conical plugging occurred on the rear surface of concrete. Different with the front steel plate, the destructive mode of the rear steel plate was like petals as shown in Fig. 8(a). The von-Mises stress contour exhibiting circular distribution and the minimum principal strain representing the compressed zone were clearly observed in Fig. 8. The rear steel plate effectively confined the rear cater to prevent the pulverized concrete fragments flying away.

As shown in Fig. 9(a), the residual velocity increased for thicker front steel plate SCS structure when the striking velocity was close to ballistic limit [12]. As the striking velocity increases, the projectile residual velocity showed a slight oscillating character. Fig. 9(b) depicted the residual velocities for 200, 250 and 300 mm thickness concrete slabs against 675 m/s striking velocity. It was also found that the rear steel

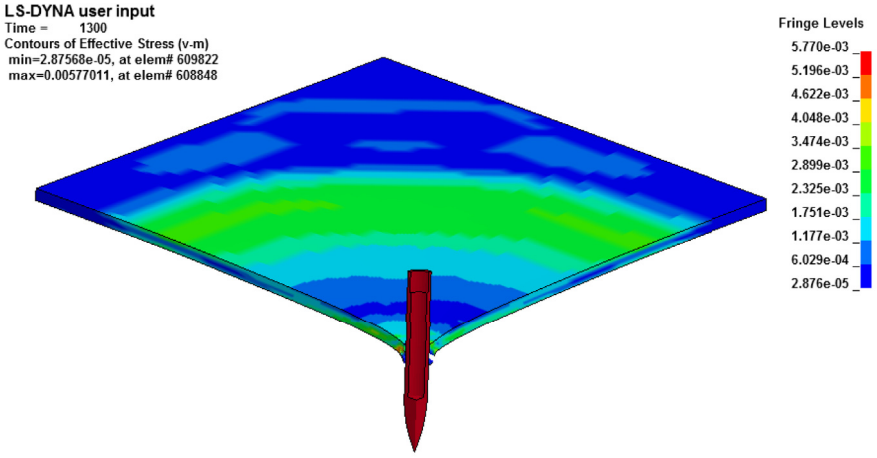

(a) Von-Mises stress distribution in rear steel plate

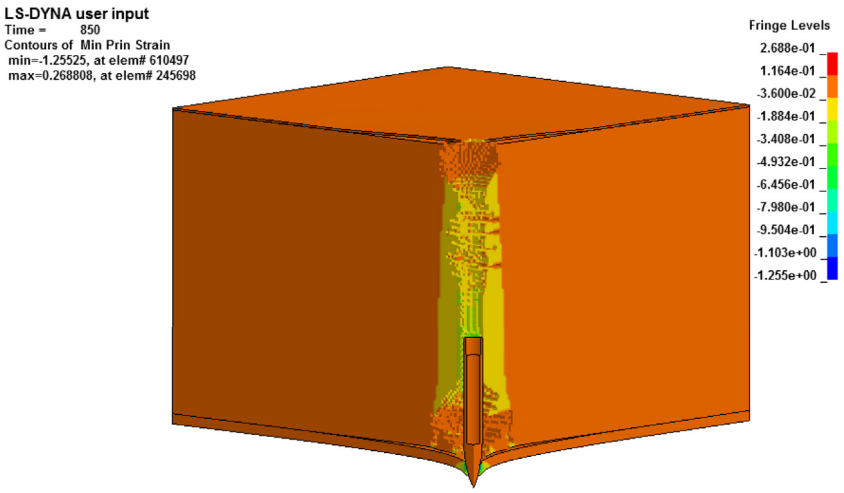

(b) Minimum principal strain distribution in SCS sandwich panels

Fig. 8. Impact response of SCS sandwich panels.

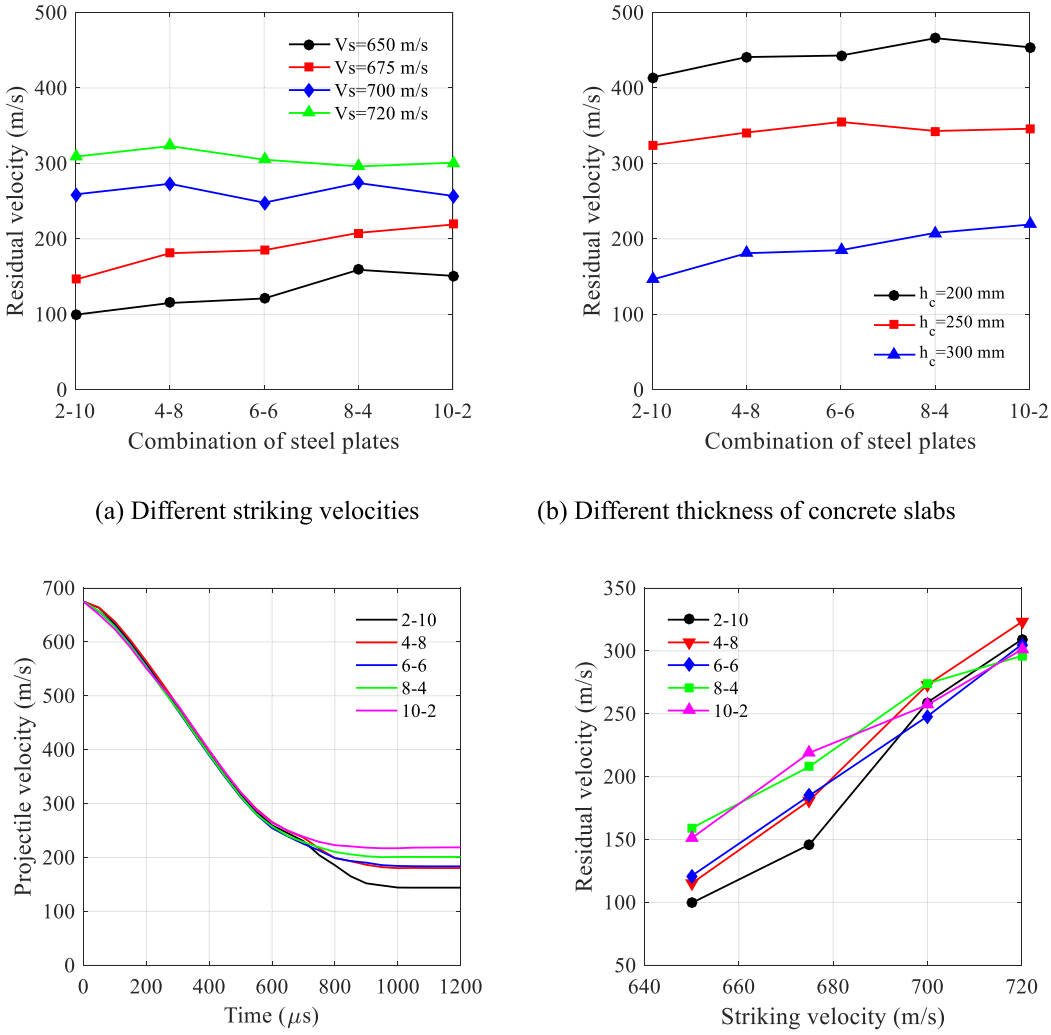

(a) Different striking velocities (b) Different thickness of concrete slabs

(c) Projectile velocity evolution over time (d) Residual velocity with different striking velocities

Fig. 9. Results of simulation on steel plate combination effect.

plate could better resist the projectile impact. It was obvious that thinner concrete slabs correspond to higher residual velocities. Under 675 m/s striking velocity, projectile velocity histories during perforating SCS sandwich panels with 300 mm thickness concrete slab was plotted in Fig. 9(c). No large difference occurred to the early penetration stages. The reason for the convergence lay in the fact that the thickness of front steel plate has much less influence on impact resistance. However, it was found that the rear steel plate has a greater effect on residual velocity. Fig. 9(d) showed the relationship between the striking velocities and the residual velocities after perforation of the SCS sandwich panels with 300 mm thickness concrete slab. For higher striking velocities, the combinations of steel plates posed less pronounced effects on the impact resistance.

4. Analytical model of SCS sandwich panels perforation

A simple but robust analytical model based on spherical cavity expansion theory and the petal-shaped destruction of thin steel plate was

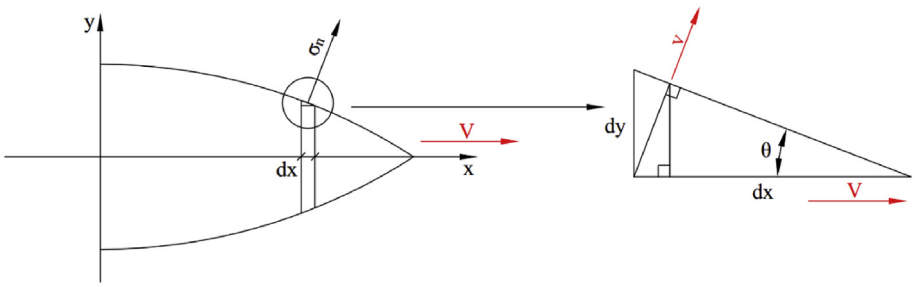

Fig. 10. Projectile nose resistance analysis.

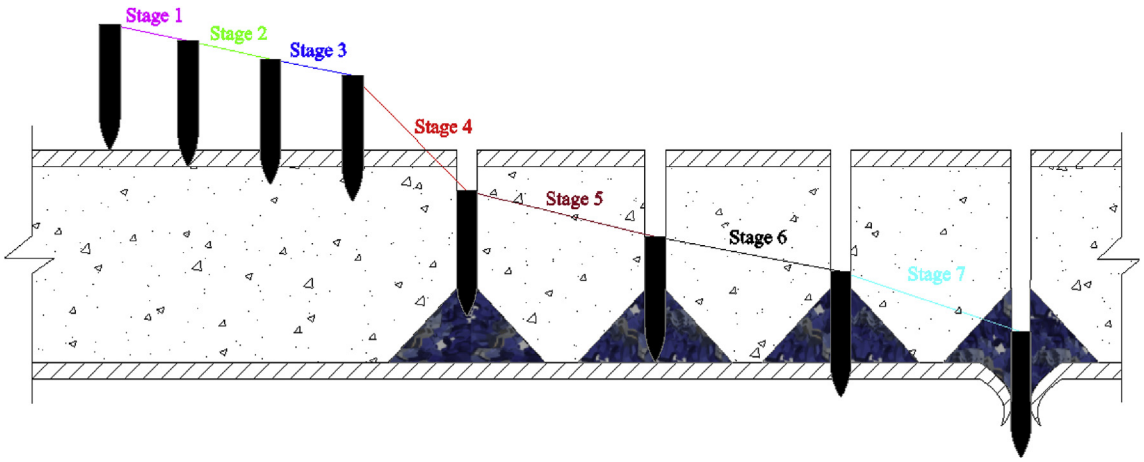

Fig. 11. Seven stages of the perforation process.

put forward in this section. The cavity expansion analysis firstly was introduced by Bishop et al. [31] to analyze the indentation mechanism. By solving the equations governing the cavity expansion process of spherical and cylindrical cavities in an elasto-plastic incompressible solid, Forrestal and his co-workers [32–34] developed the dynamic cavity expansion analysis in concrete. As mentioned previously, the perforation damage mode of the thin steel plate was generally petalling which has been numerically observed in Fig. 5(b). The petalling theory proposed by Wierzbicki [35] might be a proper solution for the rear steel plate perforation analyses.

4.1. Penetration resistance

4.1.1. Penetration in thick target

The typical ogival nose of the projectile is depicted in Fig. 10 where the length and diameter of the nose are noted as h and D. For the projectile with the velocity V, the normal velocity perpendicular to the nose surface curve is v ($v = Vsin\theta$). Denoting k as the slope of the curve and the dx is the length of micro segment. For the infinite projectile nose surface ds, the resistant force df can be regarded as the projection of the normal stress σ_n along the projectile axial direction:

$$df = \sigma_n sin\theta ds \tag{1}$$

By integrating the normal stress σ_n acting on the projectile nose, the resulting axial penetration resistant force can be expressed as:

$$F = \int \sigma_n sin\theta ds \tag{2}$$

$$ds = 2\pi|y|\sqrt{1+|k|}dx \tag{3}$$

For thick concrete slabs, Forrestal model [1,34], derived from empirical formula $S = 82.6(f_c^{'})^{-0.544}$, was adopted herein to describe the static resistant stress, and the normal resistance can be expressed as: $\sigma_n = Sf_c^{'} + \rho v^2$, where $f_c^{'}$ is the unconfined cylinder compressive strength of concrete and ρ is the density of concrete.

For thick steel plate, Rosenberg and Dekel [36] investigated the penetration on thick metal targets by simulation and they found that for low impact velocities, the deceleration of the projectiles is practicably constant, depending only on the strength of the target and the nose shape of the projectile. Above the critical impact velocity, projectile deceleration becomes velocity dependent due to the inertial response of the target. The resistant force acting on the projectile nose part can be expressed by the form:

$$F = \frac{\pi D^2}{4}\left(A_1 Y + c\rho_t v^2\right) \tag{4}$$

$$A_1 = \frac{2}{3}\left(1 + ln\left(\frac{E}{3(1-\upsilon)Y}\right)\right) \tag{5}$$

where Y is yield strength, A_1 and c are empirical factors, ρ_t is the density of steel plate, E is the Young's modulus of metal target and υ is Poisson's ratio. In this work, the investigated striking velocities were lower than the critical impact velocity, so the resistant force $F = (\pi D^2)A_1 Y/4$ and the normal resistant stress $\sigma_n = A_1 Y$.

4.1.2. Perforation on thin metal plate

The common failure modes for metal targets are: petalling, ductile failure, plugging and discing, etc. [37–40]. Usually, one of them is dominant while the others are negligible. Under rigid projectile normal penetration, the perforation damage mode of the thin metal target is generally petalling, if the ratio of the metal thickness b target and the projectile diameter D is no larger than 0.5 ($b/D \leq 0.5$) [35,40].

Impacting the target with striking velocity V_s, the projectile perforates the thin metal plate with residual velocity v_r. The initial kinetic energy of the projectile can be divided into two parts: the remaining kinetic energy of the projectile; and the energy dissipated by the thin steel plate. In the perforation process, the energy dissipation consists of elastic deformation, plastic deformation, crack propagation and expansion, thermal heating, and stress wave propagation etc. The steel plate plastic deformation is the main energy dissipation, while the other energy consumptions are much less important [37]. For the perforation process, the plastic deformation of the target plate can be divided into the deformation of remaining part and local deformation of the contact region [39]. Based on energy conservation and ignoring the secondary energy dissipation, the minimum perforation energy E_c can be expressed as:

$$E_c = W_L + W_G \tag{6}$$

where W_L is the local (petalling) energy consumption and W_G is the remaining part plastic deformation energy of the thin metal plate.

According to Wierzbicki [34], the petalling energy consumption for perforation of steel liner with thickness $b \leq 0.5D$, can be express by:

$$W_L = 3.37\sigma_0 \bar{\delta}^{0.2} b^{1.6} D^{1.4} \tag{7}$$

$$\sigma_0 = \sqrt{\frac{\sigma_y \sigma_u}{1+p}}, \quad \bar{\delta} = \frac{\delta_t}{b}, \quad \delta_t = \frac{R}{\sqrt{3}\sigma_u} \tag{8}$$

where σ_0 is flow stress, b is the thickness of thin metal plate, σ_y is the

yield stress, σ_u is ultimate strength of the steel, p is hardening exponent, δ_t is crack tip opening displacement parameter (CTOD) which takes the number of the edges of the petalling into account [40], $\overline{\delta}$ is dimensionless CTOD parameter and R is impact toughness.

The deformation energy consumption of the remaining part is quite complicated. The model proposed by Landkof and Goldsmith [41] is very complex and difficult to formulate and calculate. In order to simplify the calculation, equations (6) and (7) can be rewritten into a dimensionless form [40], and E_c can be expressed as:

$$E_c = W_L + W_G = 3.37\sigma_0\overline{\delta}^{0.2} b^{1.6} D^{1.4} + \alpha\sigma_0 D^3 \left(\frac{b}{D}\right)^{\beta} \tag{9}$$

where α and β are constants derived by data fitting. The mean resistant force $F_{mean} = \frac{E_c}{d}$ was introduced to analyze this process, where d is the actual perforation distance interaction with the rear steel plate which will be discussed in the next section.

4.2. Seven stages of SCS perforation

From the destructive mode of SCS sandwich panels, 7 stages semi-empirical analytical model is proposed which is shown in Fig. 11. Stage 1 represents the projectile penetrating the front steel plate before contacting with the concrete whereby the thickness of the steel plate is assumed to be constant. Stages 2 and 3 are featured by projectile nose contacting front steel plate and concrete at the same time. Both front plate resistance and concrete drag force contribute to the penetration resistant force. Projectile nose completely enters the concrete in stage 4. Meanwhile, stage 5 illustrates the occurring of concrete slab rear surface shear plugging until the projectile hits the rear steel plate. Stage 6 is the scenario that the projectile hits the steel plate and the pulverized concrete, simultaneously. Part of the projectile nose suffers pulverized concrete resistance while some other part interacts with the rear steel plate. This stage ends as projectile nose completely enters the rear steel plate. The last stage corresponds to the projectile only penetrates the steel plate until it totally perforates the structure. The specific mechanical analysis for each stage is as follows.

For stage 1 to stage 4, the projectile penetrates the front steel plate, concrete slab or both of them. The deep penetration model [42] is utilized to analyze the penetration in front steel plate and concrete slab. For projectile nose penetrating the front steel plate, the normal resistant stress σ'_{n,b_1} can be expressed as:

$$\sigma'_{n,b_1} = \phi\sigma_n \tag{10}$$

Considering the free-surface of front steel plate, ϕ is assumed as 0.4 in this work [43]. For the #1006 steel, Young's modulus $E = 206\ GPa$, Poisson's ratio $\upsilon = 0.29$ and yield strength $Y = 285\ MPa$. Equation (10) can be calculated as:

$$\sigma'_{n,b_1} = \phi A_1 Y = 0.4 \times \frac{2}{3}\left(1 + ln\left(\frac{E}{3(1-\upsilon)Y}\right)\right) \times Y = 518.9\ MPa \tag{11}$$

Due to the effect of the front steel plate, the front crater of concrete slab can be ignored. For projectile nose penetrating the concrete slab, the normal stress $\sigma_{n,c}$ can be expressed as:

$$\sigma_{n,c} = Sf'_c + \rho v^2 \tag{12}$$

where $f'_c = 41\ MPa$, $\rho = 2240\ \mathrm{kg/m^3}$, the static term of the normal stress $Sf'_c = 82.6 \times (f'_c/10^6)^{-0.544} \times f'_c = 449.17$ MPa.

Stage 5 indicates that the projectile passes through the pulverized concrete. As rear steel plate thickness increases, the pulverized concrete in the rear crater gets more support and becomes more effective on resisting the projectile. Practically, there is a deformation in rear steel plate, which becomes slighter as the rear steel plate becomes thicker. It is assumed that the thickness of pulverized concrete keeps constant and the density of pulverized concrete remains constant. From previous experimental tests and simulations [8,44–46], we suppose that the height of pulverized concrete $H_{p,r} = 2.5D$. According to Forrestal [47] and Shi et al. [48], the penetration model based on spherical cavity expansion analysis needs to be modified for the penetration in pulverized concrete. Because of the decayed static resistance, the normal resistant stress $\sigma'_{n,c}$ of the pulverized concrete is assumed as:

$$\sigma'_{n,c} = F\left(\frac{b_2}{D}\right) Sf'_c + \rho v^2 \tag{13}$$

where $F\left(\frac{b_2}{D}\right)$ is the modification function since the rear thickness b_2 as well as projectile diameter D are supposed to affect the penetration resistance of pulverized concrete in SCS structure. If no rear steel plate exists, the pulverized concrete pieces still pose some static resistance to the projectile, thus the modification formula should include a small constant. In absence of a better rationality, the form of $F\left(\frac{b_2}{D}\right) = \left(0.1 + 0.5\frac{b_2}{D}\right)$ is proposed by fitting the theoretical analysis projectile deceleration with the numerical result.

For stage 6 and stage 7, the projectile passes through the pulverized concrete and rear steel plate. There is a significant deformation in rear steel plate, and the destructive mode of the rear steel plate is like foregoing petals. In this section, the mean resistant force is noted as F_{mean}, and the penetration distance is assumed to be $d = b_2 + 1.5h$. In order to obtain E_c, steel plates with thickness of 2, 4, 6, 8 and 10 mm are numerically studied. For #1006 steel material, $\sigma_y = 285\ MPa$, $\sigma_u = 330\ MPa$, $p = 0.36$ and $R = 27\ J/cm^2$, and constants $\alpha = 1.07$ and $\beta = 1.04$ can be derived by data fitting from Equation (9).

The detailed resistant force for the 7 stages can be expressed as:

stage 1:

$$F_1 = \int \sigma'_{n,b_1} sin\theta ds \quad (0 < \mathrm{DOP} < b_1) \tag{14}$$

stage 2:

$$F_2 = \int \sigma'_{n,b_1} sin\theta ds + \int \sigma_{n,c} sin\theta ds \quad (b_1 < \mathrm{DOP} < h) \tag{15}$$

stage 3:

$$F_3 = \int \sigma'_{n,b_1} sin\theta ds + \int \sigma_{n,c} sin\theta ds \quad (h < \mathrm{DOP} < h + b_1) \tag{16}$$

stage 4:

$$F_4 = \int \sigma_{n,c} sin\theta ds \quad (h + b_1 < \mathrm{DOP} < b_1 + h_{2c} - 2.5D) \tag{17}$$

stage 5:

$$F_5 = \int \sigma'_{n,c} sin\theta ds \quad (b_1 + h_c - 2.5D < \mathrm{DOP} < b_1 + h_c) \tag{18}$$

stage 6:

$$F_6 = F_{mean} + \int \sigma'_{n,c} sin\theta ds \quad (b_1 + h_c < \mathrm{DOP} < b_1 + h_c + h) \tag{19}$$

stage 7:

$$F_7 = F_{mean} (b_1 + h_c + h < \mathrm{DOP} < b_1 + h_c + 1.5h) \tag{20}$$

For the projectile perforating the SCS sandwich panels with 300 mm thickness concrete slab and 10-2 combination of steel plates, the resistant force of the projectile with 675 m/s striking velocity is shown in Fig. 12. The 7 different stages are plotted in different colors. It worth noting that a sudden impulse occurs at the beginning of stage 6, which is due to the greater impact resistance to the projectile when hitting the harder rear steel plate.

4.3. Analytical model validation

The SCS sandwich panels with 300 mm thickness concrete slab and 2-10 combination of steel plates were selected to validate the analytical

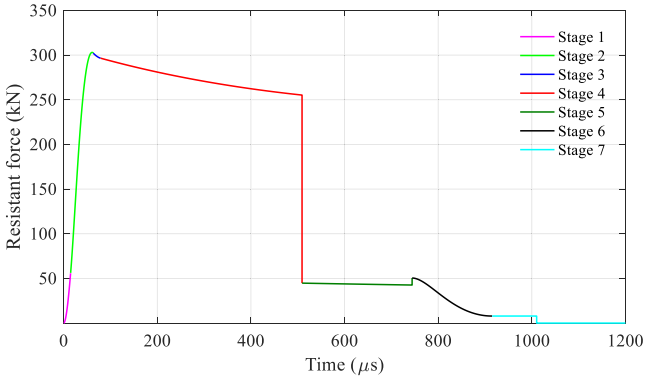

Fig. 12. Resistant force of the 7 stages.

model against numerical results whereas the projectile striking velocity was 675 m/s. The history of projectile displacement, velocity and deceleration were shown in Fig. 13(a–c). It was observed that the analytical model has good consistency with numerical results in terms of projectile deceleration evolution and residual velocity. As shown in Fig. 13(c), both analytical model and simulation captured the sudden deceleration impulse which happened around 700 μs. The reason was due to the fact that the projectile hits the rear steel plate posing greater impact resistance. Fig. 13(d) compared the numerically and analytically obtained residual velocities for 675 m/s striking velocity projectile penetrating SCS sandwich panels with 200, 250, 300 mm thickness concrete slabs pinched by steel plates. Good agreement was achieved which validates the analytical model for cases with different thickness concrete slabs. The detailed values of residual velocity were comparably listed in Table 6 whereas all the errors were within 10%.

4.4. SCS structural effect on perforation response

For the SCS sandwich panels with 300 mm thickness concrete slab, the relationship between the striking velocities and residual velocities was explored herein considering different combinations of steel plates. In Fig. 14(a), it was worth noting that the 5 curves tend to converge with the striking velocity increasing. The absorbed energy of SCS sandwich panels with 300 mm concrete slab and different combination of steel plates was plotted in Fig. 14(b). It was indicated that the absorbed energy by the sandwich structure increases as the striking velocity increases and the structure with thicker rear steel plate shows a better energy absorbing capacity. Under different striking velocities, all energy absorption curves had the tendency of linear decrease.

The effect of concrete slab thickness on the absorbed energy was also investigated. The absorbed energy of SCS sandwich panels with different

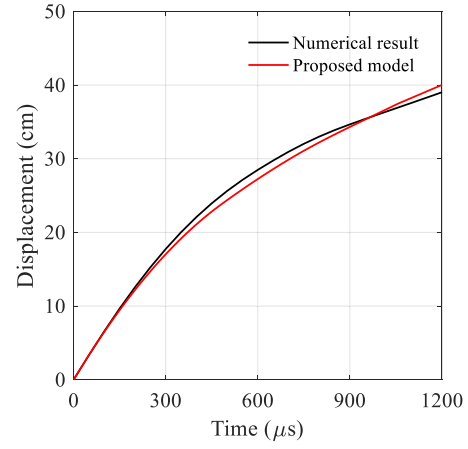

(a) Projectile displacement history

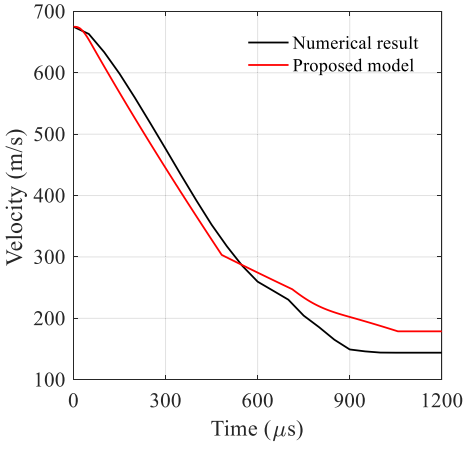

(b) Projectile velocity history

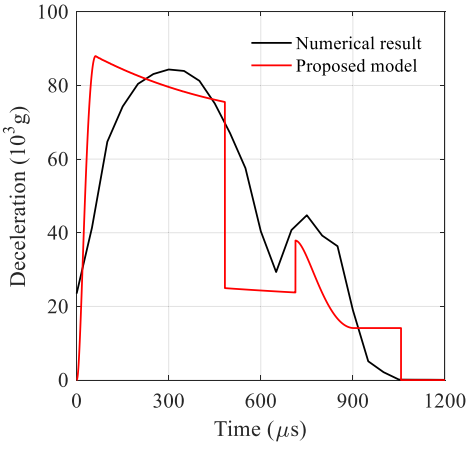

(c) Projectile deceleration history

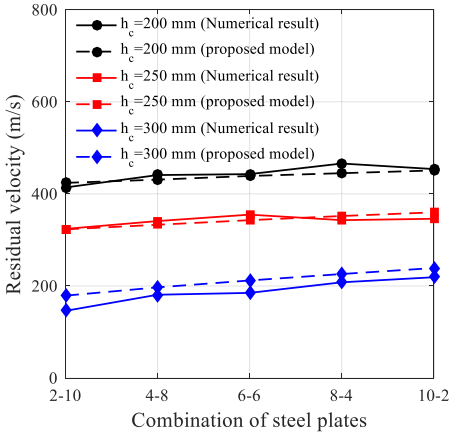

(d) Residual velocity for different SCS sandwich panels.

Fig. 13. Comparison between analytical model and simulation.

Table 6
Residual velocity of analytical model and simulation.

Combination of steel plates	h_c = 200 mm			h_c = 250 mm			h_c = 300 mm		
	$V_{r,s}$ (m/s)	$V_{r,a}$ (m/s)	Deviation	$V_{r,s}$ (m/s)	$V_{r,a}$ (m/s)	Deviation	$V_{r,s}$ (m/s)	$V_{r,a}$ (m/s)	Deviation
2–10	414	424	3.83	324	323	−0.28	146	179	6.24
4–8	441	431	−4.27	341	333	−2.40	181	197	3.24
6–6	443	439	−1.72	355	343	-.375	185	212	5.51
8–4	466	446	−9.57	343	352	2.71	208	226	3.84
10–2	454	451	−1.36	346	360	4.25	219	139	4.39

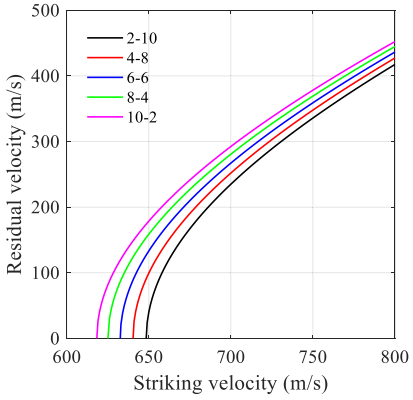

(a) Residual velocities versus striking velocities

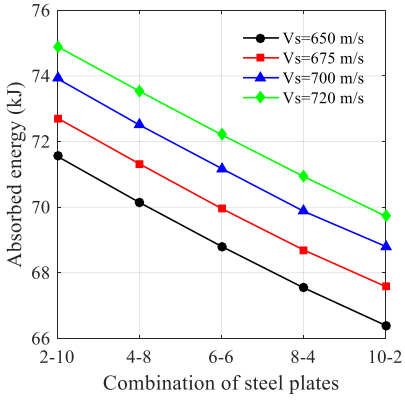

(b) Absorbed energy under different striking velocities

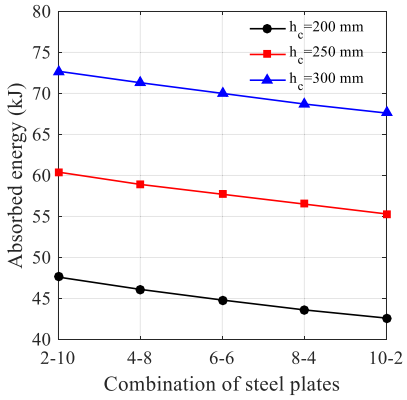

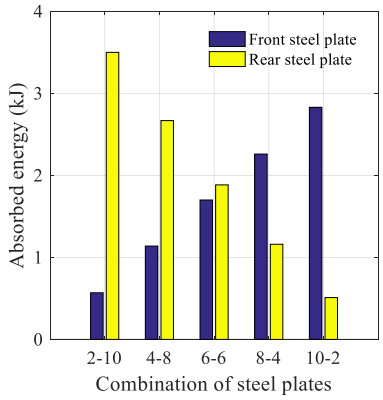

(c) Absorbed energy of different thickness concrete slabs (d) Absorbed energy by front and rear steel plates

Fig. 14. Results of analytical model.

concrete slabs was depicted in Fig. 14(c). Energy consumptions of front and rear thin steel plates were given in Fig. 14(d) for the SCS sandwich panels with 300 mm thickness concrete slab penetrated by 675 m/s projectile striking velocity. 2-10 combination of steel plates exhibited the best energy absorption capability, i.e., the energy consumption increased with the rear steel plate thickness increasing. For 6-6 combination of steel plates, the front steel plate consumes less energy than the rear steel plate. The rear steel liner were found to be more efficient in resisting the projectile impact than the front steel plate which coincides with the experimental observation by Hashimoto et al. [49].

5. Conclusions

The impact resistance of SCS sandwich panels with different thickness concrete slabs and combinations of steel plates was investigated in this work. Based on the validated numerical model of concrete-steel perforation, the SCS sandwich panels perforation was numerically studied for the structural effects. The sequent analytical model is developed with cavity expansion analysis for concrete penetration and plates petalling theory for rear steel perforation. The following conclusions can be drawn out. (1) The rear steel plate poses a significant effect on the shear plugging of concrete rear surface by arresting the pulverized concrete flying away. (2) For same thickness, the rear steel plate poses more resistance to the projectile which thus leads to smaller residual velocity, especially when the striking velocity is close to ballistic limit. (3) For high striking velocity, the projectile velocity history shows a slightly oscillating character whereby the combination of steel plates effect is less significant. (4) Based on spherical cavity expansion analysis and petelling of thin steel plate, the analytical model for hard projectile perforation on SCS sandwich panels can be validated against the numerical results. (5) With same total thickness, SCS sandwich panels structure consisting of thicker rear steel plate consumes the more energy than the ones with thicker front steel plate.

Credit author statement

Jun Feng: Writing - original draft, Data curation. Weibing Li: Visualization, Supervision. Chufan Ding: Data curation. Dacheng Gao: Visualization. Ze Shi: Writing -review & editing. Jianguo Liang: Funding acquisition.

Declaration of competing interest

The authors declare that they have no known competing financial interests or personal relationships that could have appeared to influence the work reported in this paper.

Acknowledgments

This study was supported by the National Natural Science Foundation of China (No. 11902161). Jun Feng thanks the Natural Science Foundation of Jiangsu Province (No. BK20170824). Weibing Li thanks Open Cooperative Innovation Fund of Xi'an Institute of Modern Chemistry (No. 11902161).

References

[1] A.S. Herrmann, P.C. Zahlen, I. Zuardy I, Sandwich structures technology in commercial aviation, in: Sandwich Structures 7: Advancing with Sandwich Structures and Materials, Springer, Dordrecht, 2005, pp. 13–26.
[2] J. Liew, T. Wang, Novel steel-concrete-steel sandwich composite plates subject to impact and blast load, Adv. Struct. Eng. 14 (4) (2011) 673–687.
[3] T. Abirami, G. Murali, K.S.R. Mohan, M.P. Salaimanimagudam, P. Nagaveni, P. Bhargavi, Multi-layered two stage fibrous composites against low-velocity falling mass and projectile impact, Construct. Build. Mater. 248 (2020) 118631.
[4] J.E. Crawford, S. Lan S, Blast Barrier Design and Testing. Structures Congress 2006, Structural Engineering and Public Safety, 2006, pp. 1–10.
[5] A.M. Remennikov, S.Y. Kong, Numerical simulation and validation of impact response of axially restrained steel-concrete-steel sandwich panels, Compos. Struct. 94 (2012) 3546–3555.
[6] A.M. Remennikov, S.Y. Kong, B. Uy, The response of axially restrained non-composite steel-concrete-steel sandwich panels due to large impact loading, Eng. Struct. 49 (2013) 806–818.
[7] J. Liew, K. Sohel, C.G. Koh, Impact tests on steel–concrete–steel sandwich beams with lightweight concrete core, Eng. Struct. 31 (9) (2009) 2045–2059.
[8] H. Wu H, Q. Fang, Y. Peng, Z.M. Gong, X.Z. Kong, Hard projectile perforation on the monolithic and segmented RC panels with a rear steel liner, Int. J. Impact Eng. 76 (2015) 232–250.
[9] G.I. Ofoegbu, B. Dasgupta, K.J. Smart, Fracture-based mechanical modeling of concrete, Results Eng. 6 (2020) 100107.
[10] J. Feng, W. Sun, L. Wang, L. Chen, S. Xue, W. Li, Terminal ballistic and static impactive loading on thick concrete target, Construct. Build. Mater. 251 (10) (2020) 118899.
[11] S. Inazumi, A. Jotisankasa, K. Nakao, S. Chaiprakaikeow, Performance of mechanical agitation type of ground-improvement by CAE system using 3-D DEM, Results Eng. 6 (2020) 100108.
[12] A. Remennikov, Y.K. Sih, B. Uy, Static and Dynamic Behaviour of Non-composite Steel-Concrete-Steel Protective Panels under Large Deformation, 2010.
[13] J.C. Bruhl, A.H. Varma, W.H. Johnson, Design of composite SC walls to prevent perforation from missile impact, Int. J. Impact Eng. 75 (2015) 75–87.
[14] K.S. Kim, I.H. Moon, H.J. Choi, D.W. Nam, A preliminary study on the local impact behavior of steel-plate concrete walls, Ann. Nucl. Energy 102 (2017) 210–219.
[15] J. Feng, W.W. Sun, Z.L. Liu, C. Cui, X.M. Wang, An armour-piercing projectile penetration in a double layered target of ultra-high-performance fiber reinforced concrete and armour steel: experimental and numerical analyses, Mater. Des. 102 (2016) 131–141.
[16] W. Zhao, Q. Guo, Experimental study on impact and post-impact behavior of steel-concrete composite panels, Thin-Walled Struct. 130 (2018) 405–413.
[17] J. Feng, M.L. M. Song, Q. He, W. Sun, L. Wang, K. Luo, Numerical study on the hard projectile perforationon RC panels with LDPM, Construct. Build. Mater. 183 (2018) 58–74.
[18] N.A. Dancygier, Effect of reinforcement ratio on the resistance of reinforced concrete to hard projectile impact, Nucl. Eng. Des. 172 (1997) 233–245.
[19] J. Feng, X. Gao, J. Li, H. Dong, Q. He, J. Liang, W. Sun, Penetration resistance of hybrid-fiber-reinforced high-strength concrete under projectile multi-impact, Construct. Build. Mater. 202 (2019) 341–352.
[20] K. Roy, T.C.H. Ting, H.H. Lau, J.B.P. Lim, Experimental and numerical investigations on the axial capacity of cold-formed steel built-up box sections, J. Constr. Steel Res. 160 (2019) 411–427.
[21] J. Zhang, B. Young, Compression tests of cold-formed steel I-shaped open sections with edge and web stiffeners, Thin-Walled Struct. 52 (2012) 1–11.
[22] K. Roy, C. Mohammadjani, J.B.P. Lim, Experimental and numerical investigation into the behaviour of face-to-face built-up cold-formed steel channel sections under compression, Thin-Walled Struct. 134 (2019) 291–309.
[23] F. Zhang, L.H. Poh, M.H. Zhang, Critical parameters for the penetration depth in cement-based materials subjected to small caliber non-deformable projectile impact, Int. J. Impact Eng. 137 (2020) 103471.
[24] J. Feng, M. Song, W. Sun, L. Wang, W. Li, W. Li, Thick plain concrete targets subjected to high speed penetration of 30CrMnSiNi2A steel projectiles: tests and analyses, Int. J. Impact Eng. 122 (2018) 305–317.
[25] G.R. Johnson, S.R. Beissel, T.J. Holmquist, et al., Computed radial stresses in a concrete target penetrated by a steel projectile, WIT Trans. Built Environ. 35 (1970).
[26] G.R. Johnson, A constitutive model and data for materials subjected to large strains, high strain rates, and high temperatures, in: Proc. 7th Inf. Sympo. Ballistics, 1983, pp. 541–547.
[27] C.F. Zhao, J.Y. Chen, Y. Wang, Damage mechanism and response of reinforced concrete containment structure under internal blast loading, Theor. Appl. Fract. Mech. 61 (2012) 12–20.
[28] M. Yu, X. Zha, J. Ye, The influence of joints and composite floor slabs on effective tying of steel structures in preventing progressive collapse, J. Constr. Steel Res. 66 (2010) 442–451.
[29] X. Wang, Adiabatic shear localization for steels based on Johnson-Cook model and second-and fourth-order gradient plasticity models, J. Iron Steel Res. Int. 14 (2007) 56–61.
[30] G. Ren, H. Wu, Q. Fang, Parameters of Holmquist–Johnson–Cook model for high-strength concrete-like materials under projectile impact, Int. J. Protect. Struct. 8 (3) (2017) 352–367.
[31] R.F. Bishop, R. Hill, N.F. Mott, The theory of indentation and hardness tests, Proc. Phys. Soc. 57 (3) (1945) 147–159.
[32] Forrestal M J, Tzou D Y, A spherical cavity-expansion penetration model for concrete targets. Int. J. Solid Struct. 34(31–32): 4127-4146.
[33] M.J. Forrestal, V.K. Luk, Dynamic spherical cavity-expansion in a compressible elastic-plastic solid, J. Appl. Mech. 55 (1988) 275–279.
[34] D.J. Frew, S.J. Hanchak, M.L. Green, Penetration of concrete targets with ogive-nose steel rods, Int. J. Impact Eng. 21 (1998) 489–497.
[35] T. Wierzbicki, Petalling of plates under explosive and impact loading, Int. J. Impact Eng. 22 (1999) 935–954.
[36] Z. Rosenberg, E. Dekel, The penetration of rigid long rods - revisited, Int. J. Impact Eng. 36 (2009) 551–564.
[37] J. Radin, W. Goldsmith, Normal projectile penetration and perforation of layered targets, Int. J. Impact Eng. 7 (1988) 229–259.
[38] G.G. Corbett, S.R. Reid, W. Johnson, Impact loading of plates and shells by free-flying projectiles. A review, Int. J. Impact Eng. 18 (1996) 141–230.
[39] N.K. Gupta, R. Ansari, S.K. Gupta, Normal impact of ogive nosed projectiles on thin plates, Int. J. Impact Eng. 25 (2001) 641–660.
[40] Z.G. Jiang, S.Y. Zeng, J.P. Zhou, Analysis on energy dissipation of thin metallic plates struck by rigid sharp-nosed projectiles, Acta Armamentarii 25 (2004) 777–781.
[41] B. Landkof, W. Goldsmith, Petalling of thin, metallic plates during penetration by cylindro-conical projectiles, Int. J. Solid Struct. 21 (1985) 245–266.
[42] J. Feng, W. Li, X. Wang, M. Li, H. Ren, W. Li, Dynamic spherical cavity expansion analysis of rate-dependent concrete material with scale effect, Int. J. Impact Eng. 84 (2015) 24–37.
[43] Y.K. Xiao, H. Wu, Q. Fang, A rigid projectile perforation model for metallic targets with the free-surface and fracture effects, Int. J. Protect. Struct. 8 (2017) 109–124.
[44] Y. Peng, H. Wu, Q. Fang, A note on the deep penetration and perforation of hard projectiles into thick targets, Int. J. Impact Eng. 85 (2015) 37–44.
[45] J. Li, Z. Lv, H. Zhang, Perforation experiments of concrete targets with residual velocity measurements, Int. J. Impact Eng. 57 (2013) 1–6.
[46] J.S. Hanchak, M.J. Forrestal, R.E. Young, Perforation of concrete slabs with 48 MPa (7 ksi) and 140 MPa (20 ksi) unconfined compressive strengths, Int. J. Impact Eng. 12 (1992) 1–7.
[47] M.J. Forrestal, Penetration into dry porous rock, Int. J. Solid Struct. 22 (1986) 1485–1500.
[48] C. Shi, M. Wang, L. Jie, A model of depth calculation for projectile penetration into dry sand and comparison with experiments, Int. J. Impact Eng. 73 (2014) 112–122.
[49] J. Hashimoto, K. Takiguchi, K. Nishimura K, Experimental study on behavior of RC panels covered with steel plates subjected to missile impact, in: Proceedings of 18th International Conference on Structural Mechanics in Reactor Technology, 2005.